

<https://doi.org/10.1038/s44310-024-00026-5>

# Semiconductor core fibres: a scalable platform for nonlinear photonics

Check for updates

Meng Huang<sup>1</sup>, John Ballato<sup>2</sup> & Anna C. Peacock<sup>1</sup> ✉

Semiconductor core, glass cladding fibres that can be produced with scalable dimensions and unique waveguide designs are offering new opportunities for nonlinear photonics. This paper reviews developments in the fabrication and post-processing of such semiconductor core fibres and their enabling of low loss and high efficiency nonlinear components across wavelengths spanning the near- to mid-infrared. Through adaptation and expansion of the production processes, routes to new core materials are being opened that could extend the application space, whilst all-fibre integration methods will result in more robust and practical semiconductor systems. Through continued improvement in the core materials, fibre designs and transmission losses, semiconductor fibres are poised to bring unique functionality to both the fibre and semiconductor research fields and their practical application into a myriad of optoelectronic devices.

Nonlinear semiconductor photonics is a rapidly growing field of research and application. The combination of the tight mode confinement and the high nonlinear refractive indices available in these materials allows for very compact and efficient device development<sup>1–3</sup>. Further, a wide range of semiconductor materials have been utilized for nonlinear signal processing, giving access to different optical transmission regions<sup>4</sup> and nonlinear susceptibilities, to enable either second<sup>5</sup> or third order processes<sup>6</sup>. Regardless of the choice of semiconductor, the majority of work in this field has made use of integrated on-chip platforms, primarily because of the optimized materials production methods (growth and deposition) for the planar formats<sup>7</sup>. Access to high quality materials is particularly important for the realization of low loss waveguides that are essential for nonlinear processing, which has led to a focus on Group IV semiconductors. Capitalizing on the excellent quality and the broad wavelength coverage offered by the Group IV materials, numerous nonlinear processes and demonstrations of device functionality have been reported, including optical signal processing<sup>8</sup> and source generation in silicon<sup>9,10</sup>, all-optical modulation in germanium<sup>11</sup>, frequency comb generation in silicon nitride<sup>12</sup>, and supercontinuum generation in silicon-germanium<sup>13</sup>, for example.

However, there are challenges to fabricating and working with the planar waveguides, particularly those with nanoscale dimensions, that still require some attention. Firstly, as the waveguides are formed by lithography and etching, the surface quality of the side walls can be difficult to control, and the nanoscale roughness values that are typical of most etch processes can result in sizable scattering losses at the high index contrast core/cladding boundaries<sup>14</sup>. Secondly, owing to the size-mismatch between nanoscale waveguides and micron-sized optical fibres, it is difficult to achieve efficient and robust coupling between the two platforms. This is particularly true for

use in nonlinear applications where the coupling must support relatively high pump powers and broad operating bandwidths, so that end-fire coupling is really the only viable option<sup>15,16</sup>. Although inverse tapers have been developed for low loss coupling within the telecom band<sup>17</sup>, they are not suitable for mid-infrared systems when silica cladding glasses are used, and also require very precise fabrication and alignment.

Over the past decade, semiconductor core optical fibres have emerged as an interesting alternative for the development of nonlinear semiconductor devices. Semiconductor fibres retain many of the advantageous properties of the fibre platform such as durability, polarization insensitivity, pristine core/cladding interfaces, and potential to access long waveguide lengths<sup>18</sup>. However, compared with traditional silica fibres, the semiconductor cores bring benefits of the on-chip systems such as the tight light confinement, so that they can be scaled to sub-micrometre dimensions, and the high nonlinear refractive indices reduce the power requirements of the nonlinear systems. Moreover, as semiconductors usually have much broader transmission windows than silica, semiconductor core fibres can extend the operation wavelength of fibre-based nonlinear systems from the near-infrared into the mid-infrared region<sup>1</sup>. Further, and notably, semiconductor fibres are now principally fabricated using conventional fibre drawing methods, with the high drawing speeds allowing for the rapid production of many hundreds of metres of fibre to ensure low costs and high yields of the in-fibre devices<sup>19,20</sup>. Through careful consideration of the draw parameters and the starting material, fibres can be produced with a wide range of unary and compound semiconductor cores<sup>21</sup>. Yet, the production of these waveguides is not without its own challenges, and it is generally harder to control the crystalline alignment of the semiconductor core phase during the draw process, with the as-drawn fibres being polycrystalline<sup>22</sup>.

<sup>1</sup>Optoelectronics Research Centre, University of Southampton, Southampton SO17 1BJ, UK. <sup>2</sup>Centre for Optical Materials Science and Engineering Technologies and Department of Materials Science and Engineering, Clemson University, Clemson, SC 29634, USA. ✉e-mail: [acp@orc.soton.ac.uk](mailto:acp@orc.soton.ac.uk)

It can also be difficult to achieve the continuous nanoscale core dimensions desired for many nonlinear processes due to capillary instabilities in the draw<sup>23</sup>. However, taking advantage of the robust fibre cladding, well-established fibre post-processing techniques can be exploited to optimize the core materials and achieve dimensions down to the nanoscale to not only enhance the nonlinear efficiency, but also improve the coupling to other fibre and on-chip systems.

In this paper, we review recent developments in the fabrication and post-processing techniques that have enabled the production of semiconductor core fibres that support efficient nonlinear processing. In particular, we describe the variety of materials that are compatible with the thermal drawing process and the advantages that the fibre systems offer over planar production methods. Following a review of the nonlinear processes that have been observed in the semiconductor fibres extending from the telecom band up into the mid-infrared, some perspective will be provided on the possibility to expand the application potential via access to new fibre materials and fully integrated systems. Through continued advancement of the fibre materials and processing techniques, we anticipate that these fibres will open up new avenues of exploration for semiconductor nonlinear photonics.

## Fabrication procedures

### Molten core drawing method

To date, there have been several approaches employed to fabricate semiconductor optical fibres. Chronologically, the first was the micro-pull-down method, which realized the first silicon fibres in 1996<sup>24</sup>. The second, starting in 2006, employed high-pressure chemical vapour deposition (HP-CVD) inside of a prefabricated glass capillary that subsequently acted as the fibre cladding<sup>25</sup>. The third, in 2008, was a variant of the core suction method but using a pressured (instead of evacuated) melt to flow into a capillary<sup>26</sup>. Two weeks later in 2008, the first use of the molten core method (MCM, also sometimes referred to as the “melt-in-tube” method) to semiconductor core fibres was published<sup>19</sup>. Lastly, a “reactive” approach to semiconductor phase formation was reported (first in 2011) whereby other phases are employed as precursors that react during fibre formation to yield the desired core phase<sup>27–29</sup>. Of these, only optical transmission has been reported for fibres fabricated via HP-CVD, pressurized filling, and the MCM. A series of review articles over the course of the past decade provides evolving details on each approach and their relative advantages and disadvantages<sup>18,21,30</sup>.

For the purposes of this article, the MCM will be the focus. This is because, of the noted fabrication approaches, only the MCM relies on the thermal drawing of glass. This inherently makes the MCM a more scalable approach, permitting continuous fibre fabrication at higher speeds and over long (>100 s of metre and longer) lengths<sup>31</sup>. As a result, it has become the principal method of semiconductor and multi-material fibre fabrication<sup>32–36</sup>.

The MCM was originally developed to fabricate fibres with cores that were not sufficiently stable to first form into a glass and draw<sup>37,38</sup>. The approach employs a glass cladding tube that is closed at one end and then filled with a precursor phase that melts at the draw temperature of the glass cladding. A canonical case applicable here is silicon (Si), with a melting temperature of about 1414 °C, sleeved and drawn in a pure silica glass tube at a temperature of about 1950 °C<sup>19</sup>. As discussed in greater detail in ref. 37, the generalized MCM has been applied to a wide range of glassy and crystalline core phases, in addition to the crystalline nonlinear semiconductor cores discussed herein. A schematic of the MCM is provided in Fig. 1. Similar to traditional fibre drawing, it includes a coating process to improve the mechanical strength<sup>39</sup>. A key benefit of this approach to semiconductor waveguide fabrication is that the core/cladding surfaces are defined by the atomically smooth silica glass tubing<sup>40</sup>, which helps to minimize scattering losses at the high index contrast boundary, of particular significance for waveguides with nanoscale dimensions.

Though conceptually straightforward, as with any natural process, thermodynamics and kinetics always create limitations. For example, while amorphous cores are quite common when the MCM is applied to oxide systems (including with crystalline precursors<sup>37</sup>), as-drawn semiconducting,

i.e., semi-metal cores are always fully crystalline. This contrasts with HP-CVD, which can yield either crystalline or amorphous semiconductor core fibres<sup>41</sup>. A second important natural consequence of processing materials above their melt temperature is the propensity for the melt to corrode the crucible in which it is contained. In the case of the MCM, the core melt dissolves in some components of the softened glass cladding at temperatures approaching the draw temperature. Indeed, this is what partly contributes to the formation of glassy cores in many molten core oxide systems. For the semiconductors, where crystallization kinetics are many times faster than the fibre draw speed and associated solidification rates, the dissolution of silica into silicon, for example, leads to scattering inclusions and thus increased losses. Dissolution and the accompanying diffusion are both thermally driven processes that seek to reduce a compositional gradient (i.e., silicon core, silica cladding). Accordingly, drawing at higher temperatures to fibres of smaller core sizes always promotes greater concentrations of cladding species in the core phase<sup>42</sup>. However, for nonlinear optics, small core sizes are highly desirable, if not wholly required, making thermodynamics the enemy of optical performance. Unsurprisingly then, amongst the first optimization efforts that followed the materials discovery phase of molten core semiconductor fibre development were approaches to mitigate cladding dissolution into the core. These activities focused on reactive chemistries, first “after-the-fact” by reacting away cladding oxides in the core melt<sup>43</sup> and then by proactively limiting the ingress from the initiating<sup>23</sup>. The interfacial modifier method by Gibson, et al.<sup>23</sup> is arguably amongst the most important material and process advances in the practicality of semiconductor optical fibres fabricated via conventional draw towers. However, even more recently, it has been shown that swapping the usual thermal furnace with a laser heat source reduces the heating time before drawing, allowing for the production of small core (1.3 µm diameter) silicon fibres with minimal cladding ingress<sup>49</sup>. With or without the interfacial modifier to mitigate cladding dissolution into the core, the cladding glass chemistry is also very important as it contributes significantly to the draw temperature, thermal expansion mismatch (hence residual stresses), and which species are present for contaminating the core. Cladding glasses employed for the molten core fabrication of semiconductor optical fibres include to-date silica<sup>19,23</sup>, borosilicate<sup>44,45</sup>, and phosphate<sup>46,47</sup> glasses as well as proposals for property-matched heavy metal oxides and chalcogenides<sup>48</sup>.

The MCM has enabled the realization of a vast variety of crystalline semiconductor fibre core phases. Of these materials, the Group IV core phases are by far the most well-studied and developed<sup>19,23,29,43,44,48–50</sup>. The principal reasons for such a focus are several-fold and include (i) relative simplicity of the core phase (e.g., unary cubics), (ii) relative ease of fabrication with well-behaved core melting and solidification, and generally stable and commercially available (in most cases) cladding glasses, and (iii) great familiarity with Si and Ge, and their SiGe alloys, given their commercial ubiquity. For the most developed system, Si core in a silica glass cladding, a kilometre of fibre (125 µm outer diameter and 8–10 µm core size) is straightforward to fabricate at draw rates on the order of metres per minute. Moreover, even the first molten core Ge fibre was reported at about 250 metres, despite the fact that a less durable borosilicate glass cladding was employed and that a two-draw process was required (preform to cane, followed by cane to fibre) to limit surface crystallization of the borosilicate<sup>44</sup>. Thus, the propensity of the MCM for such large-scale waveguide production is highly beneficial for reducing costs and increasing component yields.

Beyond the Group IV core phases, several II–VI compound semiconductors were amongst the earliest to be fabricated and studied, specifically InSb, in 2010<sup>46</sup>, and GaSb, in 2013<sup>51,52</sup>. As with the Group IV phases, these antimonides are well-behaved in that they melt congruently at relatively low temperatures and with negligible vapour pressure. This latter point, negligible vapour pressure, has been a historical limitation of the MCM since the build-up of vapour in the core during preform heat-up or fibre draw can lead to the explosion of the preform. It had, until recently (2022), precluded the fabrication of semiconductor cores of desirous nonlinear (and direct bandgap) phases such as GaAs<sup>53</sup> and ZnSe<sup>54</sup>. In cases such as these, where the core phase exhibits sufficient volatility upon heat-up to

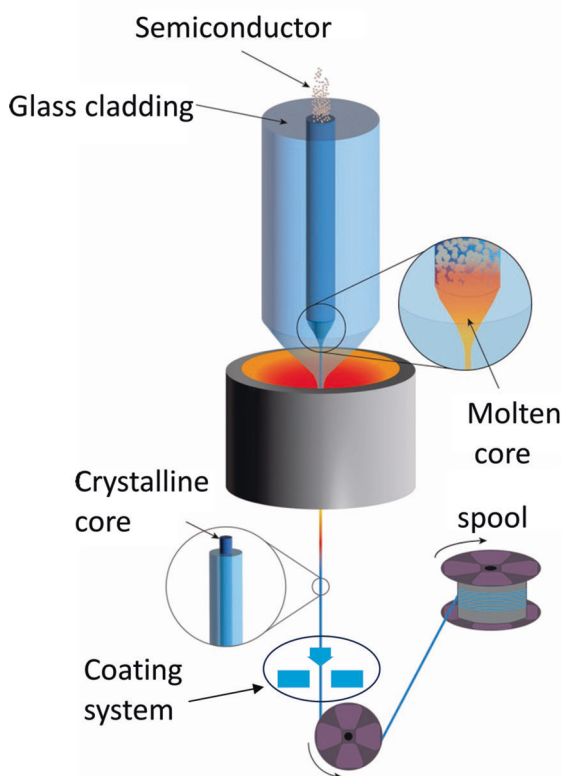


**Fig. 1** | A schematic of the molten core method for thermally drawing glass-clad semiconductor core fibres. The crystalline core is melted and encapsulated by the viscous glass cladding during the drawing process. A coating system is used to improve the mechanical strength of the produced as-drawn semiconductor core fibres.

the (cladding glass) draw temperature and/or where the core incongruently melts, the solution has been to include a low melting flux phase (i.e., “flux molten core”). The flux melts at a low temperature, dissolving the core phase into a homogeneous and low volatility liquid, which then is drawn similarly to “conventional” molten core fibre fabrication. The flux phase can be segregated away from the semiconductor phase using laser post-processing (see Section “Post-processing Techniques”). Thus, the MCM is opening a new route to the fabrication and optimization of semiconductor waveguides from materials that are not readily available in an integrated on-chip format, and which could eventually be fully incorporated within all-fibre optical and optoelectronic systems<sup>55</sup>.

As previously mentioned, the as-drawn molten core semiconductor fibres are polycrystalline. Put another way, the crystallographic orientation of the core changes discretely along the fibre. Single crystalline regions (i.e., grains) in the as-drawn fibres of several millimetres, up to approximately a centimetre, are typical. The optical isotropy of the cubic Group IV semiconductors permits light transmission even through polycrystalline cores, though scattering from impurities and defects at grain boundaries might add to loss. Not long after the noted activities to manage cladding dissolution, efforts to induce single crystallinity of the fibre cores over device-relevant lengths became active topics of study and development. The earliest approaches to promoting single crystallinity involved thermal annealing<sup>56–60</sup>. However, this was later superseded, firstly by laser heat treatments, then secondly by fibre tapering. Compared with the MCM, a key benefit of post-processing is that it is possible to apply a more precise and stable heat treatment to a selected fibre region, allowing for the formation of longer semiconductor crystal grains within the glass cladding. Thus, it is hoped that through combination of the recent advancements in the fibre

drawing methods<sup>39,50</sup> and the post-processing treatments described below, there will be a wider availability of low loss semiconductor fibres for distribution and application amongst the broader nonlinear research community.

## Post-processing techniques

### Laser processing

A schematic of laser post-processing is shown in Fig. 2a. The aim of this procedure is to heat, melt, and recrystallize the core material to grow larger polycrystalline grain sizes. The laser is focused to a small spot size by a lens, and either the laser or the fibre is scanned to control the heating and cooling dynamics of the semiconductor core, and to process longer lengths. To generate sufficient heat to melt the semiconductor, the laser wavelengths are usually selected where the core materials have strong absorption (e.g., 488 nm, 517 nm and 10.6  $\mu\text{m}$  for Si<sup>61,62</sup>, 514 nm, 632 nm and 10.6  $\mu\text{m}$  for SiGe<sup>63</sup>, 532 nm for Te<sup>32</sup>, 10.6  $\mu\text{m}$  for GaSb<sup>55,64</sup>). By placing a camera perpendicular to the laser beam, it is possible to monitor the melting and recrystallizing processes. Compared with previous thermal annealing methods (lamp-annealing<sup>56</sup>, furnace-annealing<sup>57–59</sup>), the laser heating process has many advantages. Firstly, the focused spot size is adjustable by changing the lens. Therefore, the size and position of the heating region can be more precisely controlled to be predominantly in the cladding or the core, and can even be used to generate more complex structures within the fibre (e.g. Bragg gratings<sup>65</sup>). Secondly, the laser processing has a gradient heating distribution along the radial direction in a focused beam spot. As different semiconductor materials have different solid points, this factor can be used to redistribute different components of a multi-material core fibre, making them either uniform<sup>63</sup> or segregated<sup>52,64</sup>.

The early work on laser processing was mainly focused on Si core fibres. In 2014, it was first used to engineer the bandgap of Si from 1.11 eV down to 0.59 eV by introducing an anisotropic tensile stress within a HP-CVD fibre by crystallizing the amorphous Si core to polycrystalline Si<sup>61</sup>. As the laser wavelength (488 nm) used in ref. 61 is transparent for the silica cladding, the cylindrical fibre geometry offers a unique advantage as it allows the Si core to reach a molten state, whereas the cladding is only modestly heated. As the crystalline Si core remains strongly adhered to the cladding but occupies a smaller volume than the amorphous starting material, this results in a large strain. The second, in 2016, used a CO<sub>2</sub> laser to recrystallize the poly-Si cores in MCM fibres to single-crystalline like materials through control of the cooling dynamics, thus reducing the optical loss from 14–20 dB/cm to only 2 dB/cm at 1.55  $\mu\text{m}$  and 1 dB/cm at 2  $\mu\text{m}$  wavelength<sup>62</sup>. The crystallography for the Si core after CO<sub>2</sub> laser writing was characterized by measuring the X-ray diffraction (XRD) at different positions along the fibre length, using the configuration shown in the inset of Fig. 2b. Figure 2b displays the recorded crystallographic d-spacing for both processed and unprocessed fibres, showing that the laser treatment can produce single-crystal grain sizes with lengths of more than 15 mm, highlighting the potential for the production of high quality semiconductor core fibres. Moreover, in 2017, a third body of work made use of laser processing to fabricate resonators and Bragg gratings by using the heat treatment to manipulate the core structure and glass cladding of the Si core fibres<sup>65</sup>, highlighting the flexibility to modify both the material and shape of the fibres.

Subsequent interests in laser processing then shifted to compound materials, and predominantly SiGe core fibres, which aim to extend the mid-infrared wavelength coverage over the pure Si cores<sup>66</sup>. In 2016, a CO<sub>2</sub> laser was used to homogenize the uneven segregation of Si and Ge within as-drawn SiGe core fibres, as illustrated by comparing the first two fibres in Figure 2c<sup>63</sup>. The results in ref. 63 also showed that it was possible to manipulate the positioning of the Ge content to form gratings, shown by bright sections in the third fibre in Fig. 2c, or even a graded index Ge-rich core. By exploiting this latter feature, a fibre with a Ge-rich central region (22%) within a low Ge concentration (6%) SiGe core fibre was formed in 2020, highlighting the versatility of the post-processing technique<sup>67</sup>.

Inspired by the successes of laser processing for semiconductor fibres with Group IV core materials, it was also used to engineer the optical

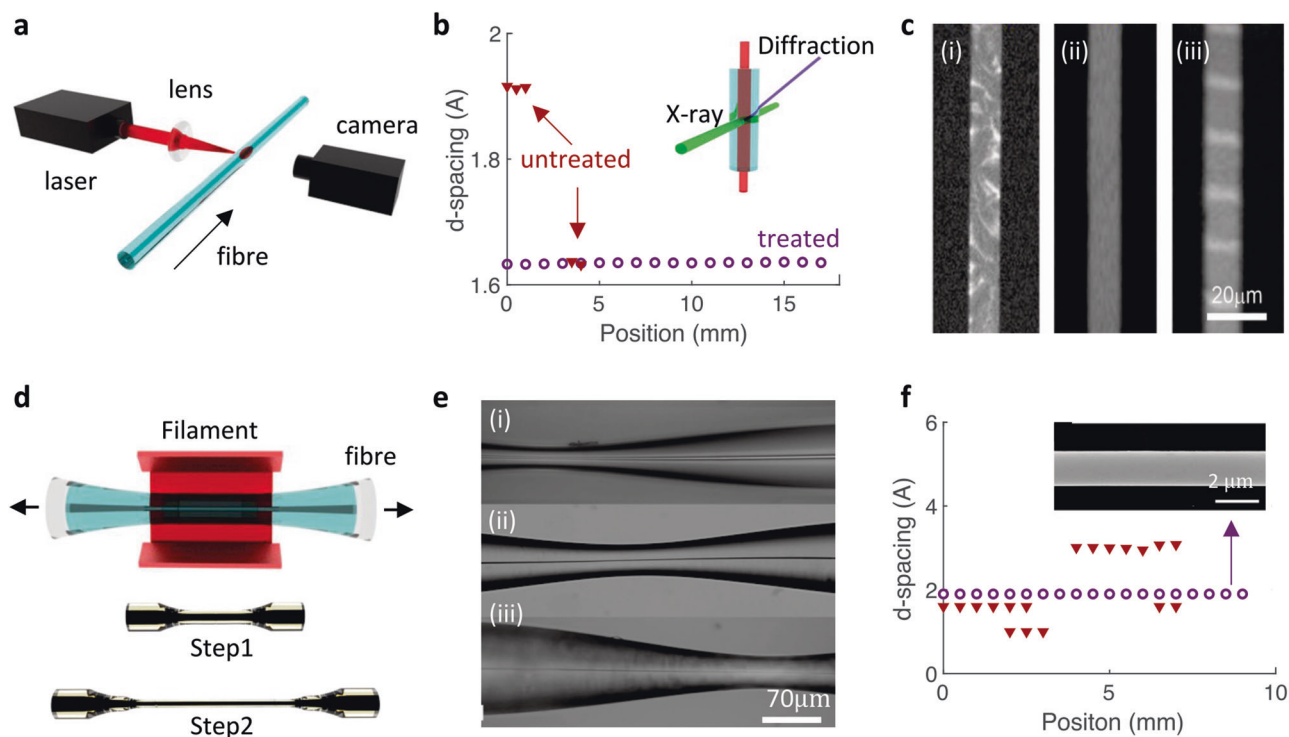


**Fig. 2 | Post-processing techniques for semiconductor core fibres.** **a** Schematic of laser processing. **b** Measured lattice spacing from X-ray diffraction as a function of position along as-fabricated and laser processed Si core fibres<sup>62</sup>. The inset shows the X-ray diffraction measurement setup. **c** Optical images of (i) an as-drawn SiGe core fibre, (ii) a laser recrystallized SiGe core and (iii) a Ge-rich grating formed within the SiGe core. **d** Schematic of the tapering procedure, showing how multiple taper steps

can be employed. **e** Images of longitudinal taper profiles for starting fibre core diameters of (i) 5.6  $\mu\text{m}$ , (ii) 2.7  $\mu\text{m}$ , and (iii) 1.3  $\mu\text{m}$ . **f** Measured X-ray diffraction along the as-fabricated and tapered Si core fibre. The inset shows an image of the smooth surface of an etched Si core fibre waist<sup>69</sup>. **c** Reproduced from ref. 63 with the permission from Springer Nature. **e** Reproduced from ref. 70 with the permission from Optica Publishing Group.

properties of fibres with other core materials, including GaSb<sup>52,64</sup> and Te<sup>32</sup>. Moreover, as previously mentioned, it is anticipated that laser processing could be used to segregate sections of pure GaAs and ZnSe core materials from the flux phases to create fibres suitable for second order nonlinear optical processing. Beyond optimization of the optical properties, laser processing has also been used to fabricate optoelectronic devices within semiconductor core fibres. In 2019, a CO<sub>2</sub> laser beam was used to segregate GaSb and Si within an as-drawn composite GaSb/Si fibre to enhance the photoluminescence<sup>68</sup>.

### Tapering

Another important post-processing method is fibre tapering. A schematic of the tapering process is shown in Fig. 2d, where a filament is used to melt the semiconductor core and soften the glass cladding. The fibre is then stretched using controllable stages to reduce the core/cladding diameters along the length. As the tapering procedure essentially mimics a second MCM draw process, importantly it provides a means to control the longitudinal profile of the fibre as well as the crystallinity. However, as the material volume is now much smaller, a lower and more controllable level of heating power can be used. To ensure the fibres have sufficient mechanical strength after being tapered to smaller sizes, the as-fabricated fibres can be sleeved inside thicker capillaries before tapering. As illustrated in Fig. 2d, two-step tapering can be used to tailor fibres with large core diameters. Compared to single-step tapering, two-step tapering can use smaller tapering ratios and lower heating powers for the final step, which is important for producing high-quality single-crystalline semiconductor cores with small diameters over long fibre lengths<sup>69</sup>.

The first tapering work was demonstrated in 2010, using a fusion splicer to adjust the core diameter of Si core fibres from 5.6  $\mu\text{m}$ , 2.7  $\mu\text{m}$  and 1.3  $\mu\text{m}$  down to waist diameters of  $\sim 3 \mu\text{m}$ ,  $\sim 2.7 \mu\text{m}$  and  $\sim 500 \text{ nm}$ , respectively<sup>70</sup>. The images of these three tapered fibres are shown in Fig. 2e. As can be seen, the tapering process produces a solid, continuous Si core

with a smooth transition from the untapered fibre to the taper waist, where at each point along the taper the core diameter changes proportionally to the changing cladding diameter. In 2012, the tapering technique was extended to tailor the core diameter of a Ge core fibre from  $\sim 150 \mu\text{m}$  to  $\sim 45 \mu\text{m}$  over a length of 16 mm, where it was shown that good control of the heating temperature (typically  $\pm 5 \text{ }^\circ\text{C}$ ) is important for increasing the single crystallinity<sup>22</sup>. However, it should be noted that no nonlinear effects were observed in refs. 22,70 due to the relatively short waist lengths ( $\sim 100 \mu\text{m}$ ) and large diameters ( $\sim 45 \mu\text{m}$ ) for the Si and Ge core fibres, respectively.

Low loss tapered Si core fibres suitable for the observation of nonlinear propagation, including nonlinear absorption and self-phase modulation (SPM), were first produced in 2016. Specifically, a submicron-sized core diameter of 0.94  $\mu\text{m}$  was achieved over a length of 1 cm, with a loss of  $\sim 3 \text{ dB/cm}$ <sup>71</sup>. XRD measurements along the tapered fibre length showed a similar level of improvement in the crystal grain size to what was seen following laser processing, as illustrated in Fig. 2f<sup>69</sup>. Thus, tapering also provides a route to producing single-crystalline like core materials. Importantly, the SEM image of an etched fibre core near the tapered waist region (inset of Fig. 2f) confirms that the surface of the core remains ultrasmooth (sub-nanometre roughness), thanks to the pristine cladding glass crucible. Thus, this serves to highlight the advantage of the fibres to achieve nanoscale waveguide dimensions with minimal loss due to surface scattering.

To date, tapering is the only post-processing method that can tailor down the MCM fibre core diameters to nanoscale dimensions ( $< 1 \mu\text{m}$ ). Although nanoscale-sized semiconductor cores can be produced directly via HP-CVD by using suitably small silica capillary templates ( $\sim 600 \text{ nm}$  in ref. 26), the deposition process is very time-consuming to achieve such small cores, the dimensions are fixed by the template, and the fibre lengths are limited to  $\leq 1 \text{ cm}$ . In contrast, the tapering technique offers a more flexible solution as the core size can be conveniently adjusted by changing the tapering ratios and the lengths are not limited by the as-drawn fibre, but only



**Table 1 | Measured optical loss (unit: dB/cm) for semiconductor core fibres that have been used for nonlinear demonstrations**

Platform	As-fabricated	Reference	Laser processed	Reference	Tapered	Reference
Si (MCM)	~10	23	2	62	0.8	88
a-Si (HP-CVD)	~50	103	1	77		
SiGe (MCM)	~20	63	12	63	2.2	76
ZnSe (HP-CVD)	1	104				
Si (MCM) <sup>a</sup>	~10	19	1	62	0.2	75
SiGe (MCM) <sup>a</sup>	~20	63	~10	63	4	76
ZnSe (HP-CVD) <sup>a</sup>	1	104				
Ge (MCM) <sup>b</sup>	~7	78	~2	78		

Top rows are for the telecom wavelength of 1.55 μm. Bottom rows for selected mid-infrared wavelengths of <sup>a</sup>~2.5 μm and <sup>b</sup>~5 μm.

the choice of tapering rig (with a tapered fibre length >6 cm being recently achieved<sup>72</sup>). Moreover, interesting fibre profiles can be fabricated with this method to enhance the functionality of the fibres. For example, in 2017, a nano-spike tip was formed by tapering the Si core to the point of collapse to form an inverse tapered coupler<sup>73</sup>, analogous to what has been used in on-chip formats<sup>74</sup>, as will be described in Section “Nonlinear Demonstrations”. Then in 2019, an asymmetric tapered fibre profile was designed to improve the output coupling of a supercontinuum generated in the mid-infrared, as detailed in Section “Optical Characterization”<sup>75</sup>. More recently tapering approaches have been applied to SiGe fibres, showing that similar materials and structural improvements can be made even in compound semiconductor systems<sup>76</sup>.

### Optical characterization

Thanks to the materials advancements associated with the laser processing and tapering procedures, several semiconductor core fibres have been produced with the low transmission losses required for nonlinear propagation. Table 1 summarizes the optical losses that have been obtained in the telecom band and at selected mid-infrared wavelengths for semiconductor core fibres that have been used for nonlinear applications. The most widely used platform has been the Si core fibres. By using laser post-processing and tapering techniques, the optical loss of MCM Si core fibres (10 dB/cm) can be reduced to 2 dB/cm and 0.8 dB/cm at a wavelength of 1.55 μm, respectively. Compared with laser post-processing, the lower losses associated with tapering can be attributed to two main reasons. Firstly, the heating zone is larger and has a more uniform temperature distribution, thus making it easier to generate a more uniform, continuous semiconductor core. Secondly, the heating zone of the filament is more stable than a focused laser beam, resulting in fewer defects. To date, the most remarkable loss reduction achieved by laser processing has been down to ~1 dB/cm at 1.55 μm wavelength in a HP-CVD amorphous Si core fibre, though the length was limited to <2 mm<sup>77</sup>.

Although less well studied, SiGe core fibres have been attracting significant attention of late due to the material’s potential for higher nonlinear coefficients and extended mid-infrared wavelength coverage in comparison to unary Si<sup>66</sup>. As the Si and Ge tend to segregate unevenly during the MCM drawing (see Fig. 2c), as-fabricated SiGe core fibres usually show very high losses (>20 dB/cm), dominated by scattering. To reduce the loss of SiGe core fibre, in 2016, laser processing was used to recrystallize the SiGe core to achieve losses of 12 dB/cm and ~10 dB/cm at 1.55 μm and ~2 μm, respectively. However, such loss values are still too high for practical use and the core diameter of the first-generation as-drawn fibres were also very large (~130 μm), precluding their use for nonlinear applications<sup>63</sup>. By employing tapering to reduce the core size and losses, these fibres have recently been produced with loss values of ~3 dB/cm for core diameters of a few micrometers<sup>76</sup>. It is worth mentioning that, in addition to the tapering discussed previously, pure Ge core fibres have also been successfully laser processed, during which the losses were reduced from ~7 dB/cm to ~2 dB/cm at wavelengths ~5 μm<sup>78</sup>.

However, the core diameters of the processed fibres (>22 μm) were too large to observe nonlinear propagation.

The only binary semiconductor fibres to be used for nonlinear demonstrations are the HP-CVD fabricated ZnSe core fibres. By optimizing the deposition recipe and temperature, these fibres could be produced with losses of only 1 dB/cm across the near-infrared and mid-infrared regimes, so that further post-processing was not required to observe nonlinear effects. However, the HP-CVD fibres are highly polycrystalline and thus it is hoped that post-processing the MCM ZnSe fibres will eventually produce fibres with higher quality core materials and controllable dimensions. Such work would be hugely significant as currently there are no practical fibres that can offer access to second order nonlinear processing.

### Nonlinear demonstrations

#### Description of nonlinear propagation

Following the realization of semiconductor fibres with losses of a few dB/cm and core diameters of a micrometre or less, it was not long before their potential for nonlinear application was demonstrated. Similar to the planar nanophotonic waveguides, pulse propagation in the semiconductor core fibres with a dominant  $\chi^3$  nonlinearity, as per the Group IV materials, can be described by the generalized nonlinear Schrödinger equation (GNLSE)<sup>79</sup>:

$$\frac{\partial A}{\partial z} = -\frac{i\beta_2}{2} \frac{\partial^2 A}{\partial t^2} - \frac{1}{2} \left( \alpha + \sigma_f + i\alpha_1 \frac{\partial}{\partial t} \right) A + i \left( \gamma + i\gamma_1 \frac{\partial}{\partial t} \right) \left( A \int_0^\infty R(t) |A|^2 dt \right) |A|^2 A. \tag{1}$$

Here  $A(z, t)$  is slowly varying pulse envelope,  $\beta_2(z)$ , is the group velocity dispersion (GVD),  $\alpha$  is the linear loss and  $\alpha_1 = d\alpha/d\omega$ .  $\sigma_f$  is the free carrier contribution and  $\sigma_f = \sigma(1 + i\mu)N_c$ , where  $\sigma$  is the free-carrier absorption (FCA) coefficient and  $\mu$  governs the free-carrier dispersion. The free-carrier density  $N_c$  is determined by the rate equation<sup>80</sup>:

$$\frac{\partial N_c(z, t)}{\partial t} = \frac{\beta_{TPA}}{2h\nu_0} \frac{|A(z, t)|^4}{A_{eff}^2} - \frac{N_c(z, t)}{\tau_c}, \tag{2}$$

where  $\tau_c$  is the estimated carrier lifetime.  $\gamma(z)$  represents the nonlinear parameter and  $\gamma_1 = d\gamma/d\omega \approx \gamma/\omega_0$ . For semiconductors, it is necessary to include both the Kerr and two-photon absorption (TPA) contributions to the nonlinearity as:  $\gamma = k_0 n_2 / A_{eff} + i\beta_{TPA} / 2A_{eff}$ , where  $\beta_{TPA}$  is the TPA coefficient,  $n_2$  is the nonlinear refractive index and  $A_{eff}$  is the effective mode area. The GNLSE also includes Raman effects, and both the electronic and vibrational contributions are included in the response function as<sup>81</sup>:

$$R(t) = (1 - f_R) \delta(t) + f_R h_R(t), \tag{3}$$

where  $f_R$  represents the fractional contribution of the delayed Raman response given by the function  $h_R(t)$ .

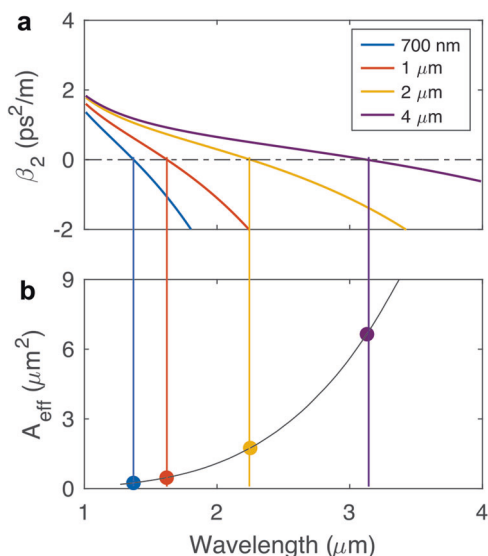


**Fig. 3 | Dispersion engineering for Si core fibres.** **a** Group velocity dispersion as a function of wavelength for different core diameters, as labelled in the legend. **b** Effective mode area variation for Si core fibres with different zero-dispersion wavelengths.

The parameters for the GNLSSE mainly depend on the waveguide material and pump wavelength. For example, the parameters for single-crystalline Si in the telecom band (e.g.,  $\lambda = 1550$  nm) are  $n_2 = 5.6 \times 10^{-18} \text{ m}^2/\text{W}$ ,  $\beta_{\text{TPA}} = 5 \times 10^{-12} \text{ m/W}$ , whilst in the mid-infrared (e.g.,  $\lambda = 3$   $\mu\text{m}$ ),  $n_2 = 3.98 \times 10^{-18} \text{ m}^2/\text{W}$  and  $\beta_{\text{TPA}}$  is negligible when operating beyond the TPA edge ( $\lambda \sim 2.2$   $\mu\text{m}$ )<sup>1</sup>. Moreover, the GVD and effective mode area, and thus  $\gamma(z)$ , depend strongly on the core diameter.

To illustrate this, Fig. 3a shows the GVD as a function of wavelength for Si core fibres with different waist diameters. As can be seen, the zero-dispersion wavelength (ZDW) shifts quite dramatically as the core is adjusted from a few microns to sub-micrometre sizes, allowing for the dispersion to be tailored for different wavelength regions, extending across the near to mid-infrared spectral bands. For example, core diameters of  $<900$  nm are required to access the anomalous dispersion regime in the telecom band, which is favoured for applications such as four-wave mixing (FWM) and soliton propagation. Figure 3b then plots the  $A_{\text{eff}}$  for the various ZDW crossings in Fig. 3a, which corresponds to the different fibre sizes. It is clear that for the larger mid-infrared fibres, the larger mode area will result in a reduced Kerr effect, though this can be compensated somewhat by the lower nonlinear losses in this region. However, another advantage of having access to large core sizes is that they can support higher power handling, and thus the nonlinear semiconductor fibre systems can be designed to deliver more practical output powers when compared to on-chip platforms.

### Telecom band applications

Owing to the ready availability of pump sources and diagnostics in the telecom band, most of the early work to characterize the nonlinear performance of the semiconductor core fibres was conducted in this wavelength region. Initially, the focus was very much on the HP-CVD fibres, as these could be produced directly with losses that were sufficiently low to observe nonlinear propagation<sup>82</sup>. However, most of this work was dedicated to characterizing the nonlinear parameters of the deposited materials<sup>82,83</sup> and, due to their relatively large core sizes, it was not possible to access the anomalous dispersion region with telecom pumps<sup>84</sup>.

However, one of the first functional demonstrations of nonlinear processing was in fact made using a HP-CVD ZnSe core fibre in 2015, as shown in the timeline of Fig. 4 ( $\chi^2$  process). In this first case, the fibre was used in a resonator geometry (15  $\mu\text{m}$  diameter core) to observe second-harmonic generation (SHG), converting the telecom pump into the visible spectrum, as illustrated in Fig. 4a<sup>85</sup>. Here the resonator helped to enhance the

light-matter interactions and obtain some phase matching between the pump and the SH. Whilst this work remains as the only demonstration of second order processes in the semiconductor core fibres, it clearly motivates the significance of obtaining high quality compound semiconductor core fibres for future applications in areas such as quantum information and imaging.

The remaining demonstrations summarized in Figure 4 ( $\chi^3$  processes), have been obtained using tapered MCM Si core fibres. Here the tapering has been critical not only for reducing the losses, but also engineering the dispersion. As a result, these fibres have allowed for the first examples of FWM processes that are used extensively in signal processing applications. In particular, in 2019, a fibre with a tapered waist of  $\sim 915$  nm (waist length 5 mm), and a loss of 2.8 dB/cm, was used as an optical parametric amplifier to generate 9 dB of gain with an average pump power of only 0.63 mW, as shown in Figure 4b<sup>86</sup>. Not only was the gain higher than what had been achieved in a similar planar silicon waveguides (5.2 dB in ref. 8), but the optimized coupling that was facilitated by the taper profile meant that this was the first example of a net parametric gain in a silicon system. Subsequently, in 2022, a similar sub-micrometre Si core fibre was used for FWM-based wavelength conversion of QPSK signals, as shown in Fig. 4c. Consistent conversion efficiencies and constellation diagrams were recorded for both C- and L-band signal wavelengths, highlighting the benefits of precise dispersion engineering for use in broadband or multi-wavelength systems<sup>87</sup>. Another noteworthy example of a FWM-based application was reported in 2023, when two identical tapered Si core fibres were fabricated (waist diameters of  $\sim 915$  nm, lengths of 1.5 cm, losses of 0.8 dB/cm) for use in an undetected-photon imaging system<sup>88</sup>. In such systems, the signal wave is used to probe the object whilst the generated idler beams, which have no interaction with the object, are used for the detection. As all the components used to construct the imaging system were fiberized, it was remarkably stable, allowing for a high degree of spatial and phase correlation, as illustrated by the amplitude image shown in Fig. 4d. Moreover, the use of FWM allows for great flexibility in the positioning of the signal and idler waves, which could potentially span both near and mid-infrared regions, presenting a unique advantage over the more traditional bulk imaging systems employing  $\chi^2$  materials<sup>89,90</sup>.

Beyond FWM, Raman scattering is another important  $\chi^3$  nonlinear process that can also be used for optical amplification or new wavelength generation. In fact, Raman scattering was the first nonlinear process to be demonstrated in planar silicon waveguide systems as, unlike FWM, it does not require phase matching<sup>91</sup>. However, owing to the relatively short lengths and high losses ( $\sim 2$  dB/cm) of the early tapered Si core fibres, Raman scattering was only recently observed in 2021. The demonstration was achieved by producing a Si core fibre with a core diameter of only 750 nm over a length of  $\sim 2$  cm, and a reduced loss of  $\sim 1$  dB/cm<sup>92</sup>. A maximum Raman gain of 1.1 dB was observed with a CW pump power of only 48 mW, as shown in Fig. 4e, comparable to planar systems with similar waveguide dimensions and pumps. Further simulations conducted using the GNLSSE (Eq. (1)) have indicated that the Raman gain could be increased substantially (up to 6 dB) by simply increasing the fibre length to  $\sim 10$  cm, highlighting the importance of obtaining longer tapered fibres in future work.

As a final demonstration, Fig. 4f shows self-phase modulation (SPM) broadening of a comb source, of potential use in wavelength division multiplexing systems. This work was reported in 2022, using a Si core fibre that was fully integrated with standard single mode fibres (SMF), as will be discussed in Section “Nonlinear Demonstrations”. Significantly, the simple use of SPM in this work helped to preserve the important comb features such as spectral flatness, low noise levels, narrow tone bandwidths and high tone powers, that are important for many communication applications<sup>93</sup>. Thus, this serves to highlight the value of having access to the full range of nonlinear processes to ensure maximal impact of the fibre systems.

### Applications into the mid-infrared

Inspired by the successes in the telecom band, recent attention has shifted to explorations in the mid-infrared spectral region where there are important

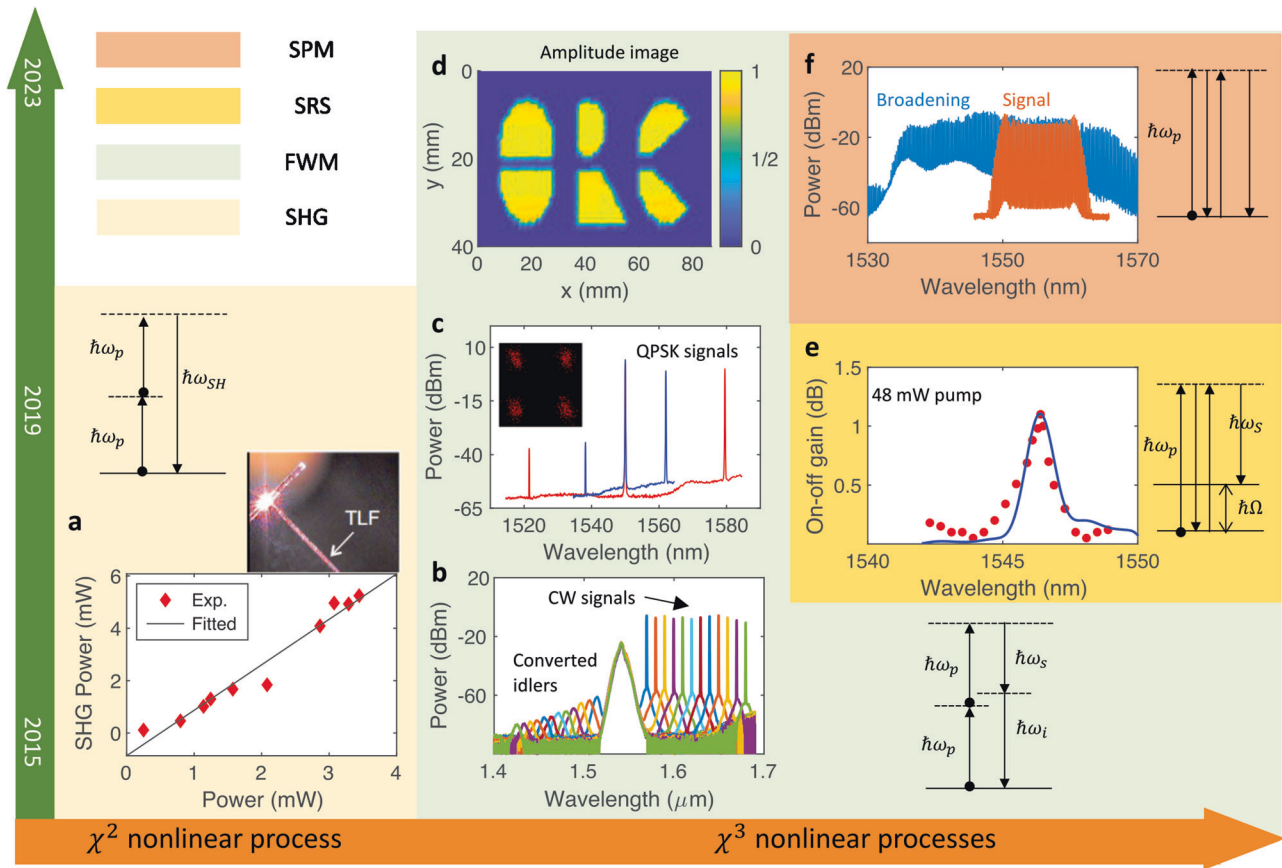


**Fig. 4 | Summary of nonlinear semiconductor core fibre devices in the telecom band. a** Second-harmonic generator. **b** Optical parametric amplifier based on FWM. **c** FWM wavelength converter, with inset showing a retrieved constellation diagram at the 1521 nm wavelength. **d** FWM-based undetected-photon imaging

system. **e** Raman amplifier. **f** Parametric mixer based on SPM as a broadband comb source. **d** Reproduced from ref. 88 with the permission from Chinese Laser Press. **f** Reproduced from ref. 93 with the permission from Springer Nature.

applications in gas sensing<sup>94</sup>, environmental monitoring<sup>95</sup>, and medical diagnostics<sup>96</sup>. In this regard, the semiconductor core fibres offer a unique advantage over their planar waveguide counterparts in that, as indicated in Fig. 3a, they can be readily produced with larger, few micron-sized cores, that are well-suited to mid-infrared operation. Moreover, when using the Si core fibres, the TPA parameter becomes negligible when operating at wavelengths >2.2 μm, so that short-pulsed lasers with high peak powers can be used to boost the nonlinear performance<sup>97</sup>. Although chalcogenides have long been a popular material of choice for mid-infrared nonlinear fibre optics owing to their broad transmission windows and low transmission losses (< 5 dB/m)<sup>98</sup>, they typically have lower nonlinear refractive indices than crystalline semiconductors (by around an order of magnitude)<sup>1</sup> and they can also suffer from stability and photosensitivity issues<sup>98</sup>. Thus, the silica-clad semiconductor core fibres offer an advantage over chalcogenide fibres in terms of their high nonlinearity, strong durability, and mechanical robustness, particularly for systems requiring short fibre lengths and high operating powers.

By further adapting the fibre tapering, it has been possible to produce long lengths of micron-sized Si core fibres with losses <1 dB/cm. Access to such low losses becomes even more important for the longer wavelength pumps due to the lower intensities associated with the larger  $A_{eff}$  also seen in Fig. 3b. Figure 5a shows results of simulations conducted using the GNLSE (Eq. (1)) indicating how the FWM conversion bandwidth depends on the core diameter for a pump positioned at ~2 μm, a typical wavelength for a thulium doped fibre laser system<sup>99</sup>. The maximum bandwidth exceeds 1200 nm for a waist diameter of 1.6 μm. By fabricating a tapered Si core fibre with the target core diameter over a length of 4 cm, and a loss of 0.5 dB/cm, an experimental conversion bandwidth of 690 nm was obtained, as shown

in Fig. 5b. It should be noted that the measured bandwidth was only limited by the tuneability of the available seed signal and the low pump power (6 dBm average power, corresponding a peak power of ~2 W).

By further extending the Si core fibre length to 6 cm and reducing the transmission loss to 0.2 dB/cm, Raman scattering and amplification was observed with the same 2 μm pump source<sup>72</sup>. A maximum time-averaged Raman gain of 3.7 dB was obtained for a pump power of 12.4 mW, as shown in Fig. 5c, corresponding to a peak on-off Raman gain of ~30 dB when considering the 125 ps pulse duration. Interestingly, because of the long pulse duration, nonlinear absorption at the 2 μm pump wavelength is still significant, so that increasing the pump power will not result in a significant increase in the Raman gain. However, if the pump could be shifted to a longer wavelength of 2.2 μm, where TPA is negligible, a significant increase in the gain can be achieved. In this case, the first Stokes wave can grow sufficiently strong to act as a seed for higher order cascaded processes, as displayed via the GNLSE simulations in Fig. 5d. Thus, this worked illustrated the potential for Si core fibres to form the basis of tuneable wavelength sources across the 2-5 μm range.

Beyond FWM wavelength conversion and Raman amplification, tapered Si core fibres have also been used for supercontinuum generation - a process that draws on all the full suite of nonlinear effects. Figure 5e shows a tapered fibre profile that was designed especially for the observation of supercontinuum generation at mid-infrared wavelengths. Particularly, the fibre had an asymmetric profile such that the long-tapered input facilitated optimum coupling into the waist, whilst the short output taper ensured minimal interaction of the newly generated long wavelength light with the lossy silica cladding<sup>75</sup>. The fabricated fibre was designed for a pump wavelength of 3 μm and had a waist diameter of 2.8 μm over a length of only



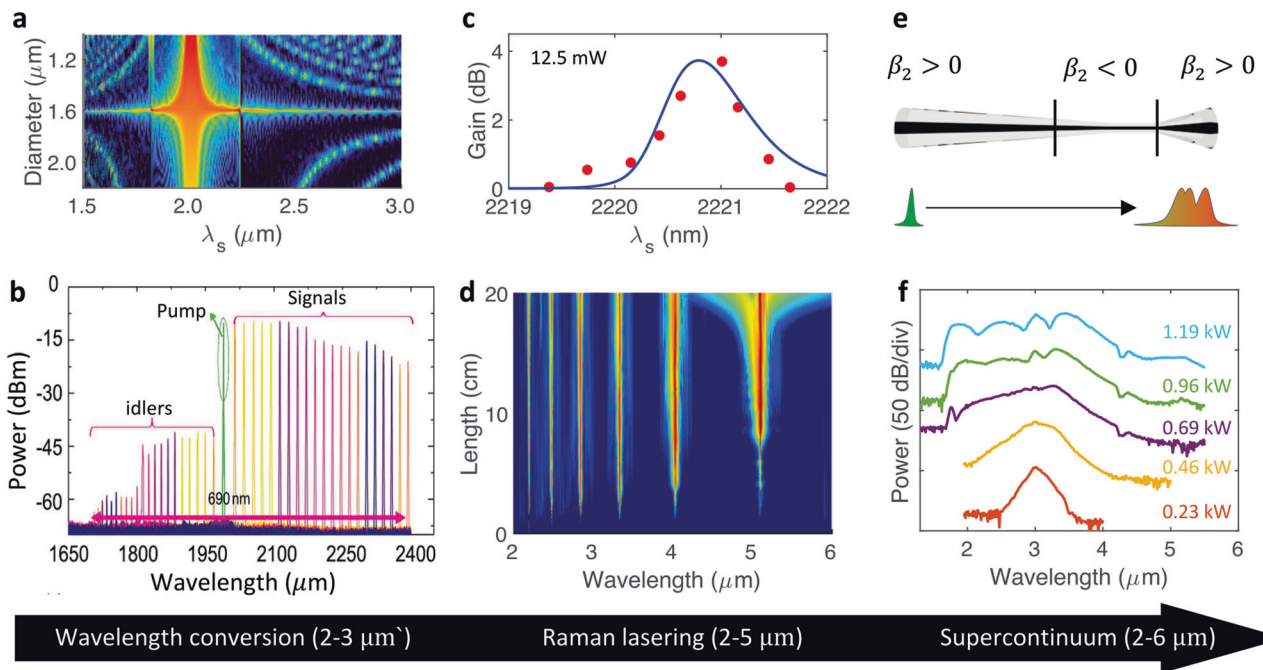


**Fig. 5 | Summary for nonlinear semiconductor core fibre demonstrations in the mid-infrared regime.** **a** Simulation results of FWM efficiency as a function of signal wavelength and Si core diameters when pumped at 2  $\mu\text{m}$ . **b** Measured mid-infrared FWM output spectra for a Si core fibre with a core diameter of 1.6  $\mu\text{m}$  over a length of 4 cm. **c** Measured average on-off Raman gain in a Si core fibre with a waist diameter of 1.59  $\mu\text{m}$  and a length of 6 cm. **d** Simulation results of cascaded Raman scattering

when pumped at 2.2  $\mu\text{m}$  wavelength with a peak power of 20 W. **e** Si core fibre profile designed for mid-infrared supercontinuum generation. **f** Measured output supercontinuum generation spectra obtained in an asymmetric tapered Si core fibre for different pump peak powers, as labelled. **a, b** Reproduced from ref. 99 with the permission from AIP Publishing. **c, d, f** Reproduced from refs. 72,75 with the permission from Springer Nature.

1.7 mm to keep the cladding absorption to a minimum, with input and output core diameters of 10  $\mu\text{m}$ . The resulting output spectra obtained with input pump powers up to  $\sim 10$  mW is shown in Fig. 5e. The broadest spectrum spans almost two octaves ( $\sim 1.7$ ), covering wavelengths from 1.62  $\mu\text{m}$  to 5.34  $\mu\text{m}$ , with the red edge of the spectrum extending well beyond what had been previously achieved in any planar silicon-on-insulator (SOI) waveguide by around 2  $\mu\text{m}$ .

Despite these achievements, mid-infrared transmission of the Si fibres will always be limited by the core transmission to wavelengths up to  $\sim 8$   $\mu\text{m}$ . However, Ge materials can offer extended transmission up to  $\sim 14$   $\mu\text{m}$  as well as higher nonlinear coefficients, so that Ge core fibres present as an interesting alternative for long wavelength source generation. As previously mentioned, although Ge core fibres have been successfully tapered and laser processed, so far their nonlinear performance has yet to be fully characterized. However, Ge core fibres have been used to demonstrate a nonlinear response from the core, firstly through Raman emission at 6.8  $\mu\text{m}$  when pumped with a QCL source at 5.6  $\mu\text{m}$ <sup>100</sup>, and secondly via the observation of detuning oscillations in the frequency-resolved response of pump probe experiments conducted at 4.6  $\mu\text{m}$ <sup>101</sup>. Thus, these works highlight the potential of these fibres for mid-infrared source generation provided the losses can be reduced from the current levels, to values closer to what has been achieved in silicon (see Table 1). Alternatively, the SiGe core fibres also offer potential to extend the operational window beyond the pure Si cores, but still retain access to the more advanced production methods that have enabled low losses. Thus, further work to optimize the core dimensions and losses of the SiGe core fibres for wavelengths  $> 2$   $\mu\text{m}$  could help open new routes to achieving high quality mid-infrared semiconductor fibres. We note that as the operating wavelengths get longer, reducing the losses due to the silica cladding may not be possible by simply altering the fibre design as in ref. 75, and alternative cladding materials may need to be considered that offer lower losses in the mid-infrared<sup>48</sup>.

## Perspective and outlook

### New materials—second order nonlinear systems

As described in Section “Fabrication Procedures”, the MCM has become the focus of semiconductor fibre fabrication, owing to its scalability and alignment with commercial fibre production methods. Through adapting the post-processing methods, there is a clear route for the optimization and nonlinear application of the SiGe and Ge fibres in the near future, which will be important for applications within the longer mid-infrared wavelength region. It is worth noting that although there is currently considerable interest within the chip-based community in other third order nonlinear materials such as silicon nitride and titanium dioxide<sup>102</sup>, principally as they offer broad transmission windows from the visible to the mid-infrared, these are not compatible with MCM due to their high melting temperatures. Thus, in terms of expanding the material systems, focusing on the development of second order core materials, e.g., GaAs<sup>53</sup> and ZnSe<sup>54</sup>, which also offer very broad transparency windows, presents the most fruitful approach for the fibre work. However, so far, the MCM fibre quality has precluded direct measurement of important optical properties, such as loss or nonlinearities, so that their maturity lags significantly behind the Si core fibres. It is, therefore, perhaps best here to muse instead on what is possible, what seemingly is not possible, and why.

From the perspective of scalable fabrication, the requirement of a (typically metal) flux to permit thermal drawing in a glass cladding mandates subsequent laser post-processing to segregate the nonlinear phase from metal. However, the more phase-pure the nonlinear phase, the more likely the issues of volatility and incongruity that restricted their “conventional” MCM fabrication. Although the high nonlinearity and tight mode confinement of the small core semiconductor fibres means that only short phase-pure sections are needed for device functionality, it may be that lateral segregation (across the core cross-section), rather than longitudinal, ends up as the more practical approach. This would be somewhat analogous to a planar waveguide inside a glass-clad, fibre core. However, one advantage of this approach is that laser drilling holes through the cladding could then



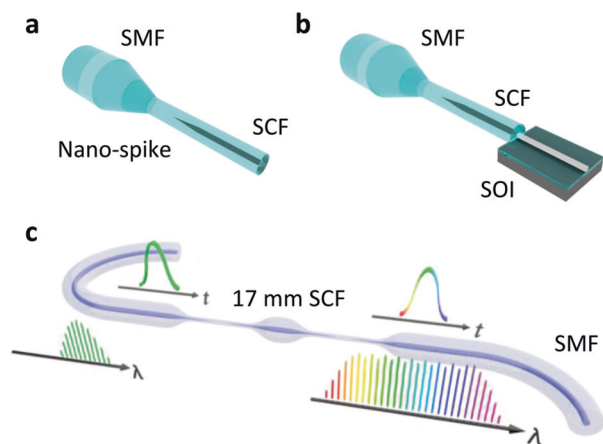


**Fig. 6 | Fibre integrated nonlinear semiconductor photonic systems.** **a** Schematic of a nano-spike coupler to enhance the coupling between SMF and a semiconductor core fibre (SCF). **b** Concept of using a Si core fibre with a nano-spike coupler to transition light from SMF to a Si-on-insulator (SOI) waveguide on-chip. **c** Schematic of an all-fibre integrated Si core fibre parametric mixer for comb source broadening in the telecom band<sup>93</sup>.

enable electrical contacts to the metal (flux) phase, thus marrying  $\chi^2$  (or  $\chi^3$ ) nonlinear functionality, with direct bandgap light emission all within a fibre platform. Whatever the final geometry, it is clear that having access to the broadest range of in-fibre semiconductor materials is important for maximizing the application potential of this platform.

### Fibre connections— all-fibre integrated systems

One of the main motivations for incorporating the semiconductor materials inside fibre geometries is the potential for seamless integration with more conventional fibre networks. Despite this promise, most of the nonlinear demonstrations described in Section “Optical Characterization” have been achieved using free space coupling systems, either using lenses or tapered lens fibres. Although the lensed fibre approach allows for high coupling efficiencies ( $\sim 3$  dB/facet) and ensures the systems are essentially all-fiberized, the connection points are not robust and still require precise alignment, limiting their portability. To achieve robust and user-friendly connections between SMF and the semiconductor core fibres, in 2019, a nano-spike coupler approach was developed to facilitate the connection, as shown in Fig. 6a. Here, the spike helps to transition the light from the low index glass core to the high index semiconductor through a graded mode conversion. The benefits of this coupler are: (i) improved mode matching between the fibres, (ii) reduced reflection losses, and (iii) robust splicing between the silica cladding structures. Although the first fabricated nano-spike coupler had a loss of  $\sim 3$  dB<sup>73</sup>, simulations of the mode coupling predict that losses of  $\sim 1$  dB are achievable with the correct fibre designs.

Moreover, these semiconductor fibre couplers could also serve as an interface between SMF and planar semiconductor waveguides, provided the fibre and planar core dimensions were well matched, as illustrated in Fig. 6b. Currently, the main challenge to the fabrication of these couplers is that the outer cladding diameter of the nano-spike region is very small ( $\sim 30$   $\mu\text{m}$ ), so the mechanical strength of coupler is not very strong<sup>73</sup>. Thus, there is work on-going to fabricate fibres with more suitable core/cladding ratios to better match both the fibre-to-fibre and fibre-to-chip interfaces. However, it is also possible to make use of capillary sleeves to support the fibres in the coupling region, similar to the role of a conventional splice protector. Using such a scheme, in 2022 a Si core fibre was pig-tailed on both ends with SMF fibres to produce an all-fibre parametric mixer, as shown schematically in Fig. 6c. The fabricated Si fibre had a core diameter of 1.1  $\mu\text{m}$  over a length of 1.7 cm, which was used to broaden the bandwidth of a frequency comb source through SPM, as shown in Fig. 4f. As previously mentioned, thanks to the relatively short length of the Si core fibre section, the key performance

metrics of the comb source required for telecommunications applications was preserved. However, the high nonlinearity of the silicon section resulted in a tripling of the comb bandwidth with only modest telecom pump powers. Thus, this work demonstrates an important step towards practical all-fibre integrated nonlinear semiconductor photonic systems.

### Conclusion

This paper has reviewed developments in the fabrication and post-processing of semiconductor core fibres that are emerging as robust and scalable platforms for nonlinear applications. These fibres are now primarily fabricated by the molten core drawing method, owing to its capacity for high speed and high-volume production, as well as its suitability for adaption to both unary and compound semiconductor core materials. When combined with post-processing methods such as laser heating and tapering, low loss fibres can be produced over lengths of several centimetres, with core dimensions that can be tailored from a few microns down to hundreds of nanometres. Through precise control of the longitudinal profile to engineer the dispersion and enhance the coupling, it has been possible to observe a wide range of nonlinear effects, starting in the telecom band and extending up into the mid-infrared regime. Moreover, with access to new materials and integration schemes starting to emerge, it is expected that these fibres will continue to expand the avenues of exploration for advanced fibre systems in terms of the available nonlinear processes and transmission windows. Although the semiconductor core fibres will not replace their chip-based waveguide counterparts, they will help to extend the rich landscape of nonlinear semiconductor photonics.

### Data availability

The data that support the findings of this study are available from the corresponding author upon reasonable request.

Received: 13 March 2024; Accepted: 6 June 2024;

Published online: 02 July 2024

### References

- Zhang, L., Agarwal, A. M., Kimerling, L. C. & Michel, J. Nonlinear Group IV photonics based on silicon and germanium: from near-infrared to mid-infrared. *Nanophotonics* **3**, 247–268 (2014).
- Vyas, K. et al. Group III-V semiconductors as promising nonlinear integrated photonic platforms. *Adv. Phys.: X* **7**, 2097020 (2022).
- Xiong, C. et al. Aluminum nitride as a new material for chip-scale optomechanics and nonlinear optics. *N. J. Phys.* **14**, 095014 (2012).
- Soref, R. Mid-infrared photonics in silicon and germanium. *Nat. Photonics* **4**, 495–497 (2010).
- Shoji, I., Kondo, T. & Ito, R. Second-order nonlinear susceptibilities of various dielectric and semiconductor materials. *Opt. Quantum Electron.* **34**, 797–833 (2002).
- Leuthold, J., Koos, C. & Freude, W. Nonlinear silicon photonics. *Nat. Photonics* **4**, 535–544 (2010).
- Koch, T. L. & Koren, U. Semiconductor photonic integrated circuits. *IEEE J. Quantum Electron.* **27**, 641–653 (1991).
- Foster, M. A. et al. Broad-band optical parametric gain on a silicon photonic chip. *Nature* **441**, 960–963 (2006).
- Salem, R. et al. Signal regeneration using low-power four-wave mixing on silicon chip. *Nat. Photonics* **2**, 35–38 (2008).
- Rong, H. et al. An all-silicon Raman laser. *Nature* **433**, 292–294 (2005).
- Shen, L. et al. Mid-infrared all-optical modulation in low-loss germanium-on-silicon waveguides. *Opt. Lett.* **40**, 268–271 (2015).
- Okawachi, Y. et al. Octave-spanning frequency comb generation in a silicon nitride chip. *Opt. Lett.* **36**, 3398–3400 (2011).
- Sinobad, M. et al. Mid-infrared octave spanning supercontinuum generation to 8.5  $\mu\text{m}$  in silicon-germanium waveguides. *Optica* **5**, 360–366 (2018).

14. Barwicz, T. & Haus, H. A. Three-dimensional analysis of scattering losses due to sidewall roughness in microphotonic waveguides. *J. Lightwave Technol.* **23**, 2719 (2005).
15. Liu, X. et al. Bridging the mid-infrared-to-telecom gap with silicon nanophotonic spectral translation. *Nat. Photonics* **6**, 667–671 (2012).
16. Wei, J. et al. Supercontinuum generation assisted by wave trapping in dispersion-managed integrated silicon waveguides. *Phys. Rev. Appl.* **14**, 054045 (2020).
17. Pu, M., Liu, L., Ou, H., Yvind, K. & Hvam, J. M. Ultra-low-loss inverted taper coupler for silicon-on-insulator ridge waveguide. *Opt. Commun.* **283**, 3678–3682 (2010).
18. Peacock, A. C., Sparks, J. R. & Healy, N. Semiconductor optical fibres: progress and opportunities. *Laser Photonics Rev.* **8**, 53–72 (2014).
19. Ballato, J. et al. Silicon optical fiber. *Opt. Express* **16**, 18675–18683 (2008).
20. McMillen, C. et al. On crystallographic orientation in crystal core optical fibers. *Optical Mater.* **32**, 862–867 (2010).
21. Gibson, U. J., Wei, L. & Ballato, J. Semiconductor core fibres: materials science in a bottle. *Nat. Commun.* **12**, 3990 (2021).
22. McMillen, C. et al. On crystallographic orientation in crystal core optical fibers II: Effects of tapering. *Optical Mater.* **35**, 93–96 (2012).
23. Nordstrand, E. F., Dibbs, A. N., Eraker, A. J. & Gibson, U. J. Alkaline oxide interface modifiers for silicon fiber production. *Optical Mater. Express* **3**, 651–657 (2013).
24. Shimamura, K., Uda, S., Yamada, T., Sakaguchi, S. & Fukuda, T. F. T. Silicon single crystal fiber growth by micro pulling down method. *Jpn. J. Appl. Phys.* **35**, L793 (1996).
25. Sazio, P. J. et al. Microstructured optical fibers as high-pressure microfluidic reactors. *Science* **311**, 1583–1586 (2006).
26. Tyagi, H., Schmidt, M., Sempere, L. P. & Russell, P. S. J. Optical properties of photonic crystal fiber with integral micron-sized Ge wire. *Opt. Express* **16**, 17227–17236 (2008).
27. Orf, N. D. et al. Fiber draw synthesis. *Proc. Natl Acad. Sci.* **108**, 4743–4747 (2011).
28. Hou, C. et al. Direct atomic-level observation and chemical analysis of ZnSe synthesized by in situ high-throughput reactive fiber drawing. *Nano Lett.* **13**, 975–979 (2013).
29. Hou, C. et al. Crystalline silicon core fibres from aluminium core preforms. *Nat. Commun.* **6**, 6248 (2015).
30. Peacock, A., Gibson, U. & Ballato, J. Silicon optical fibres—past, present, and future. *Adv. Phys.: X* **1**, 114–127 (2016).
31. Ballato, J. et al. Advancements in semiconductor core optical fiber. *Opt. Fiber Technol.* **16**, 399–408 (2010).
32. Han, B. et al. Multifunctional single-crystal tellurium core multimaterial fiber via thermal drawing and laser recrystallization. *J. Am. Ceram. Soc.* **105**, 1640–1647 (2022).
33. Yan, W. et al. Thermally drawn advanced functional fibers: New frontier of flexible electronics. *Mater. Today* **35**, 168–194 (2020).
34. Strutynski, C. et al. Co-drawing of technical and high-performance thermoplastics with glasses via the molten core method. *Sci. Rep.* **13**, 5092 (2023).
35. Kang, S., Dong, G., Qiu, J. & Yang, Z. Hybrid glass optical fibers—novel fiber materials for optoelectronic application. *Opt. Mater.: X* **6**, 100051 (2020).
36. Zhang, J., Wang, Z., Wang, Z. & Wei, L. Advanced multi-material optoelectronic fibers: a review. *J. Lightwave Technol.* **39**, 3836–3845 (2020).
37. Ballato, J. & Peacock, A. Perspective: Molten core optical fiber fabrication—A route to new materials and applications. *APL Photonics* **3**, 120903 (2018).
38. Ballato, J. & Snitzer, E. Fabrication of fibers with high rare-earth concentrations for Faraday isolator applications. *Appl. Opt.* **34**, 6848–6854 (1995).
39. Harvey, C. M., Mühlberger, K., Oriekhov, T., Maniewski, P. & Fokine, M. Specialty optical fiber fabrication: Fiber draw tower based on a CO laser furnace. *JOSA B* **38**, F122–F129 (2021).
40. Healy, N. et al. Polycrystalline silicon optical fibers with atomically smooth surfaces. *Opt. Lett.* **36**, 2480–2482 (2011).
41. Baril, N. F. et al. Confined high-pressure chemical deposition of hydrogenated amorphous silicon. *J. Am. Chem. Soc.* **134**, 19–22 (2012).
42. Cavillon, M., Dragic, P., Faugas, B., Hawkins, T. W. & Ballato, J. Insights and aspects to the modeling of the molten core method for optical fiber fabrication. *Materials* **12**, 2898 (2019).
43. Morris, S. et al. Reactive molten core fabrication of silicon optical fiber. *Opt. Mater. Expr.* **1**, 1141–1149 (2011).
44. Ballato, J. et al. Glass-clad single-crystal germanium optical fiber. *Opt. Express* **17**, 8029–8035 (2009).
45. Dmitrieva, I., Lopez-Iscoa, P., Milanese, D. & Petit, L. Ternary borosilicates as potential cladding glasses for semiconductor core optical fibers. *Int. J. Appl. Glass Sci.* **10**, 151–156 (2019).
46. Ballato, J. et al. Binary III-V semiconductor core optical fiber. *Opt. Express* **18**, 4972–4979 (2010).
47. Tang, G. et al. Phosphate glass-clad tellurium semiconductor core optical fibers. *J. Alloy. Compd.* **633**, 1–4 (2015).
48. Morris, S. et al. Cladding glass development for semiconductor core optical fibers. *Int. J. Appl. Glass Sci.* **3**, 144–153 (2012).
49. Kudinova, M. et al. Two-step manufacturing of hundreds of meter-long silicon micrometer-size core optical fibers with less than 0.2 dB/cm background losses. *APL Photonics* **6**, 026101 (2021).
50. Wang, Z. et al. High-quality semiconductor fibres via mechanical design. *Nature* **626**, 72–78 (2024).
51. Scott, B. L. & Pickrell, G. R. Fabrication of GaSb optical fibers. *Process. Prop. Adv. Ceram. Compos. V: Ceram. Trans.* **240**, 65 (2013).
52. Song, S. et al. Crystalline GaSb-core optical fibers with room-temperature photoluminescence. *Opt. Mater. Expr.* **8**, 1435–1440 (2018).
53. Zaengle, T. et al. A novel route to fibers with incongruent and volatile crystalline semiconductor cores: GaAs. *ACS Photonics* **9**, 1058–1064 (2022).
54. Zaengle, T., Martinez, E., Hawkins, T. W., McMillen, C. & Ballato, J. A novel route to fibers with volatile crystalline semiconductor cores part 2: Selenides and phosphides. *Optical Mater.* **145**, 114388 (2023).
55. Song, S. et al. Localised structuring of metal-semiconductor cores in silica clad fibres using laser-driven thermal gradients. *Nat. Commun.* **13**, 2680 (2022).
56. Gupta, N. et al. Annealing of silicon optical fibers. *J. Appl. Phys.* **110**, 093107 (2011).
57. Zhao, Z., Cheng, X., Xue, F., He, T. & Wang, T. Effect of annealing temperature on the stress and structural properties of Ge core fibre. *J. Cryst. Growth* **473**, 1–5 (2017).
58. Zhao, Z., Xue, F., Mao, Y., Chen, N. & Wang, T. Effects of annealing on the residual stresses distribution and the structural properties of Si core fiber. *Optical Fiber Technol.* **41**, 193–199 (2018).
59. Ordu, M. et al. Effect of thermal annealing on mid-infrared transmission in semiconductor alloy-core glass-clad fibers. *Adv. Fiber Mater.* **2**, 178–184 (2020).
60. Zhao, Z. et al. High temperature annealing of Si core fiber with different annealing time. *Opt. Fiber Technol.* **58**, 102288 (2020).
61. Healy, N. et al. Extreme electronic bandgap modification in laser-crystallized silicon optical fibres. *Nat. Mater.* **13**, 1122–1127 (2014).
62. Healy, N. et al. CO<sub>2</sub> laser-induced directional recrystallization to produce single crystal silicon-core optical fibers with low loss. *Adv. Opt. Mater.* **4**, 1004–1008 (2016).
63. Coucheron, D. A. et al. Laser recrystallization and inscription of compositional microstructures in crystalline SiGe-core fibres. *Nat. Commun.* **7**, 13265 (2016).

64. Liu, B. et al. Purification and single crystallization of glass-cladding GaSb core fiber using 532 nm laser-driven thermal gradients. *J. Am. Ceram. Soc.* **106**, 5078–5085 (2023).
65. Fokine, M. et al. Laser structuring, stress modification and Bragg grating inscription in silicon-core glass fibers. *Opt. Mater. Express* **7**, 1589–1597 (2017).
66. Hon, N. K., Soref, R. & Jalali, B. The third-order nonlinear optical coefficients of Si, Ge, and  $\text{Si}_{1-x}\text{Ge}_x$  in the midwave and longwave infrared. *J. Appl. Phys.* **110**, 011301 (2011).
67. Wu, W. et al.  $\text{CO}_2$  laser annealed SiGe core optical fibers with radial Ge concentration gradients. *Opt. Mater. Express* **10**, 926–936 (2020).
68. Song, S. et al. Laser restructuring and photoluminescence of glass-clad GaSb/Si-core optical fibres. *Nat. Commun.* **10**, 1790 (2019).
69. Franz, Y. et al. Material properties of tapered crystalline silicon core fibers. *Opt. Mater. Express* **7**, 2055–2061 (2017).
70. Healy, N., Sparks, J., Sazio, P., Badding, J. & Peacock, A. Tapered silicon optical fibers. *Opt. Express* **18**, 7596–7601 (2010).
71. Suhailin, F. H. et al. Tapered polysilicon core fibers for nonlinear photonics. *Opt. Lett.* **41**, 1360–1363 (2016).
72. Huang, M. et al. Raman amplification at 2.2  $\mu\text{m}$  in silicon core fibers with prospects for extended mid-infrared source generation. *Light Sci. Appl.* **12**, 209 (2023).
73. Ren, H. et al. Tapered silicon core fibers with nano-spikes for optical coupling via spliced silica fibers. *Opt. Express* **25**, 24157–24163 (2017).
74. Almeida, V. R., Panepucci, R. R. & Lipson, M. Nanotaper for compact mode conversion. *Opt. Lett.* **28**, 1302–1304 (2003).
75. Ren, H. et al. Low-loss silicon core fibre platform for mid-infrared nonlinear photonics. *Light Sci. Appl.* **8**, 105 (2019).
76. Ghosh, A. N., Huang, M., Ballato, J., Gibson, U. J., Peacock, A. C. Nonlinear optical properties of polycrystalline silicon-germanium core fibers from telecom wavelengths into the mid-infrared spectral region. *Photonics Europe*. SPIE, 13004-13031 (2024).
77. Ji, X. et al. Single-crystal silicon optical fiber by direct laser crystallization. *ACS Photonics* **4**, 85–92 (2017).
78. Zhao, Z., Zhang, J., Wang, S., Du, Y. & Ren, L.  $\text{CO}_2$  laser annealing of Ge core fibers with different core diameters. *Opt. Fiber Technol.* **66**, 102645 (2021).
79. Peacock, A. & Healy, N. Parabolic pulse generation in tapered silicon fibers. *Opt. Lett.* **35**, 1780–1782 (2010).
80. Yin, L. & Agrawal, G. P. Impact of two-photon absorption on self-phase modulation in silicon waveguides. *Opt. Lett.* **32**, 2031–2033 (2007).
81. Agrawal, G. P. In *Nonlinear fiber optics* (Springer, 2000).
82. Mehta, P. et al. Nonlinear transmission properties of hydrogenated amorphous silicon core optical fibers. *Opt. Express* **18**, 16826–16831 (2010).
83. Shen, L. et al. Nonlinear transmission properties of hydrogenated amorphous silicon core fibers towards the mid-infrared regime. *Opt. Express* **21**, 13075–13083 (2013).
84. Shen, L. et al. Four-wave mixing and octave-spanning supercontinuum generation in a small core hydrogenated amorphous silicon fiber pumped in the mid-infrared. *Opt. Lett.* **39**, 5721–5724 (2014).
85. Vukovic, N. et al. Tunable continuous wave emission via phase-matched second harmonic generation in a ZnSe microcylindrical resonator. *Sci. Rep.* **5**, 11798 (2015).
86. Wu, D. et al. Net optical parametric gain in a submicron silicon core fiber pumped in the telecom band. *APL Photonics* **4**, 086102 (2019).
87. Wu, D. et al. Four-wave mixing-based wavelength conversion and parametric amplification in submicron silicon core fibers. *IEEE J. Sel. Top. Quantum Electron.* **27**, 1–11 (2020).
88. Huang, M. et al. Classical imaging with undetected photons using four-wave mixing in silicon core fibers. *Photonics Res.* **11**, 137–142 (2023).
89. Lemos, G. B. et al. Quantum imaging with undetected photons. *Nature* **512**, 409–412 (2014).
90. Cardoso, A. C. et al. Classical imaging with undetected light. *Phys. Rev. A* **97**, 033827 (2018).
91. Claps, R., Dimitropoulos, D., Raghunathan, V., Han, Y. & Jalali, B. Observation of stimulated Raman amplification in silicon waveguides. *Opt. Express* **11**, 1731–1739 (2003).
92. Huang, M. et al. Continuous-wave Raman amplification in silicon core fibers pumped in the telecom band. *APL Photonics* **6**, 096105 (2021).
93. Sohanpal, R. et al. All-fibre heterogeneously-integrated frequency comb generation using silicon core fibre. *Nat. Commun.* **13**, 3992 (2022).
94. Willer, U., Saraji, M., Khorsandi, A., Geiser, P. & Schade, W. Near- and mid-infrared laser monitoring of industrial processes, environment and security applications. *Opt. Lasers Eng.* **44**, 699–710 (2006).
95. Du, Z., Zhang, S., Li, J., Gao, N. & Tong, K. Mid-infrared tunable laser-based broadband fingerprint absorption spectroscopy for trace gas sensing: a review. *Appl. Sci.* **9**, 338 (2019).
96. Ghorbani, R. & Schmidt, F. M. Real-time breath gas analysis of CO and  $\text{CO}_2$  using an EC-QCL. *Appl. Phys. B* **123**, 1–11 (2017).
97. Ren, H. et al. Nonlinear optical properties of polycrystalline silicon core fibers from telecom wavelengths into the mid-infrared spectral region. *Optical Mater. Express* **9**, 1271–1279 (2019).
98. Petersen, C. R. et al. Mid-infrared supercontinuum covering the 1.4–13.3  $\mu\text{m}$  molecular fingerprint region using ultra-high NA chalcogenide step-index fibre. *Nat. Photonics* **8**, 830–834 (2014).
99. Wu, D. et al. Broadband, tunable wavelength conversion using tapered silicon fibers extending up to 2.4  $\mu\text{m}$ . *APL Photonics* **8**, 106105 (2023).
100. Wang, P. et al. Mid-infrared Raman sources using spontaneous Raman scattering in germanium core optical fibers. *Appl. Phys. Lett.* **102**, 011111 (2013).
101. Ordu, M. et al. Nonlinear optics in germanium mid-infrared fiber material: Detuning oscillations in femtosecond mid-infrared spectroscopy. *AIP Adv.* **7**, 095125 (2017).
102. Brès, C.-S. et al. Supercontinuum in integrated photonics: generation, applications, challenges, and perspectives. *Nanophotonics* **12**, 1199–1244 (2023).
103. Lagonigro, L. et al. Low loss silicon fibers for photonics applications. *Appl. Phys. Lett.* **96**, 041105 (2010).
104. Sparks, J. R. et al. Zinc selenide optical fibers. *Adv. Mater.* **23**, 1647–1651 (2011).

## Acknowledgements

We would like to thank their colleagues and collaborators who contributed to the cited work, particularly Dr Dong Wu, Dr Amar Ghosh, Dr Haonan Ren, Prof. Ursula Gibson, and Thomas Hawkins, as well as Miranda Stone for rendering Figure 1.

## Author contributions

M.H., J.B. and A.C.P. prepared the manuscript text together. A.C.P. and M.H. were responsible for the figure preparation and final editing. All authors reviewed the manuscript.

## Competing interests

The authors declare no competing interests.

## Additional information

**Correspondence** and requests for materials should be addressed to Anna C. Peacock.

**Reprints and permissions information** is available at <http://www.nature.com/reprints>

**Publisher's note** Springer Nature remains neutral with regard to jurisdictional claims in published maps and institutional affiliations.



**Open Access** This article is licensed under a Creative Commons Attribution 4.0 International License, which permits use, sharing, adaptation, distribution and reproduction in any medium or format, as long as you give appropriate credit to the original author(s) and the source, provide a link to the Creative Commons licence, and indicate if changes were made. The images or other third party material in this article are included in the article's Creative Commons licence, unless indicated otherwise in a credit line to the material. If material is not included in the article's Creative Commons licence and your intended use is not permitted by statutory regulation or exceeds the permitted use, you will need to obtain permission directly from the copyright holder. To view a copy of this licence, visit <http://creativecommons.org/licenses/by/4.0/>.

© The Author(s) 2024